Bioelectrochemistry 120 (2018) 150–156

Contents lists available at ScienceDirect

Bioelectrochemistry

journal homepage: www.elsevier.com/locate/bioelechem

Rose petal and P123 dual-templated macro-mesoporous TiO_2 for a hydrogen peroxide biosensor

Xu Wu [a], Huanhuan Zhang [b], Kejing Huang [c,*], Yan Zeng [d], Zhihong Zhu [d,*]

[a] College of Physics and Electronic Engineering, Xinyang Normal University, Xinyang 464000, PR China
[b] Collaborative Innovation Center of Henan Province for Energy-Saving Building Materials, Xinyang Normal University, Xinyang 464000, PR China
[c] College of Chemistry and Chemical Engineering, Xinyang Normal University, Xinyang 464000, PR China
[d] Institute of Nano-science and Nano-technology, College of Physical Science and Technology, Central China Normal University, Wuhan, 430079, China

ARTICLE INFO

Article history:
Received 11 September 2017
Received in revised form 16 December 2017
Accepted 16 December 2017
Available online 19 December 2017

Keywords:
Electrochemical biosensor
Rose petal templates
Mesoporous TiO_2
Horseradish peroxidase
H_2O_2 detection

ABSTRACT

In this work, highly ordered macro-mesoporous TiO_2 has been successfully synthesized using fresh rose petals and P123 ($EO_{20}PO_{70}EO_{20}$) as dual templates through a simple soaking and calcining process. Characterization of the as-prepared TiO_2 indicated that the mesoporous structure of the TiO_2 was highly ordered, with a pore diameter of approximately 3 nm. After electrodeposition of Pt nanoparticles onto the TiO_2 as an electron transfer enhancer and the immobilization of horseradish peroxidase (HRP) onto the TiO_2-modified electrode, a biosensor for detecting hydrogen peroxide (H_2O_2) was realized. This biosensor showed a wide linear detection range from 5 μM to 8 mM and a low detection limit of 1.65 μM with good stability and high selectivity, suggesting that the sensor is well-suited for the detection of H_2O_2.

1. Introduction

TiO_2, an n-type semiconductor, is widely applied in catalysis [1], molecular adsorption [2], biosensing [3] and energy storage [4] due to its advantages such as high photocatalysis, nontoxicity, good biocompatibility and excellent chemical/physical stability. For sensing applications in particular, TiO_2 has been extensively studied based on its ability to exist in various morphologies, such as sol — gel matrices [5], nanotubes [6,7], nanowires [8,9], nanorods [10] and hollow microspheres [11]. Among these architectures, the mesoporous structure [12–14] has shown much promise due to its possession of a high surface area that provides more active sites for the immobilization of noble metals and biomolecules.

Recently, much attention has been directed towards the development of biotemplates, based on their low cost, nontoxicity, environmentally friendliness and extensive existence in nature. Accordingly, biotemplates have been widely used to prepare hierarchical nanomaterials for use in photocatalysis applications, supercapacitors, lithium ion batteries and biosensors. For example, morpho butterfly wings were used as biotemplates to fabricate PMAA photonic crystals with hierarchical structures [15]. Collagen fiber was also utilized to synthesize cerium-doped TiO_2 mesoporous nanofibres for photocatalysis [16]. Additionally, eggshell membrane [17], microalgae [18], regenerated cellulose membrane [19], pollen grains [20], cotton [21] and cellulose [22] have also been used as biotemplates. However, almost all biotemplates need to be pretreated under heavy acidic or alkali conditions.

Herein, fresh rose petals and P123 were used as templates to synthesize highly ordered macro-mesoporous TiO_2 by a dual-template method for use in the development of an electrochemical enzyme biosensor. Horseradish peroxidase (HRP) was also used in the construction of the biosensor. The developed method is a simple, facile and controllable synthetic process that involves only soaking and calcining, along with the use of fresh rose petals without any pretreatment beyond washing in deionized water. The macroporous structure of the as-prepared highly ordered macro-mesoporous TiO_2 was obtained from the papillae on the surface of the rose petal, which had an average diameter of 10 μm, and the mesopores were oriented by the structure-directing agent P123. These two templating agents worked together to generate the unique hierarchical macro-mesoporous structure of the product. The high biocompatibility of TiO_2 is very beneficial in maintaining the bioactivity of the HRP after its immobilization onto the biosensor. However, TiO_2 does not have good conductivity; therefore, platinum nanoparticles were introduced onto the TiO_2 electrode by electrodeposition to further enhance the direct electron transfer speed [23]. After the electrodeposition, the Pt/TiO_2-modified electrode was reacted with HRP to form a hydrogen peroxide (H_2O_2) biosensor.

* Corresponding authors.
E-mail addresses: kejinghuang@xynu.edu.cn (K. Huang), zhzhu@mail.ccnu.edu.cn (Z. Zhu).

https://doi.org/10.1016/j.bioelechem.2017.12.009
1567-5394/

Cyclic voltammetry and chronoamperometry methods were used to investigate the direct electrochemical and electrocatalytic behaviours of the prepared biosensor. The results of these tests demonstrated that the fabricated biosensor possessed a wide linear detection range from 5 μM to 8 mM and a low detection limit of 1.65 μM. The sensor also displayed good stability and high selectivity. These attributes suggested great potential for use of the developed biosensor in the detection of H_2O_2. Two primary biological factors played key roles in this study. First, the natural morphological features of rose petals were explored for use as hard templates in the synthesis of the nanomaterial. Then, the properties of the obtained nanomaterial were exploited to develop a biosensor through the immobilization of an enzyme (in this case HRP, though other enzymes could also be used) onto the macro-mesoporous TiO_2.

2. Experimental

2.1. Reagents and instrumentation

Horseradish peroxidase (>250 U mg^{-1}) and P123 (M 5800) were obtained from Sigma-Aldrich. Tetrabutyl titanate and $H_2PtCl_6 \cdot 6H_2O$ were purchased from Sinopharm Chemical Reagent Co., Ltd. Acetylacetone was purchased from Tianjin Fuchen Chemicals Reagent Factory. The supporting electrolyte was a 0.1 M phosphate buffer solution (PBS, pH 7.0). All chemicals used in this work were of analytical grade.

All electrochemical measurements were carried out on a CHI electrochemical workstation (Shanghai CH Instrument, CHI 440A, China) with a three-electrode system consisting of an HRP-modified electrode as the working electrode, a platinum wire as the counter electrode and a saturated calomel electrode (SCE) as the reference electrode. Ultraviolet-visible (UV–vis) light absorption spectra were collected on a Shimadzu spectrophotometer (Shimadzu UV-1700, Japan). Fourier transform infrared (FT-IR) spectroscopy was performed on a Nicolet spectrophotometer (Nicolet Company, 5700 FT-IR, America). Scanning electron microscopy (SEM) was performed on a JSM-6700F instrument (JEOL, Japan), with all samples metalized by coating with Au and immobilized onto dark conducting resin prior to analysis. X-ray powder diffraction (XRD) patterns were collected on an X'Pert PRO MRD (PANalytical, Netherlands).

2.2. Synthesis of macro-mesoporous TiO_2

Macro-mesoporous TiO_2 was synthesized by a dual-template method using fresh rose petals and P123 [24]. First, P123, ethyl alcohol and hydrochloric acid were added to deionized (DI) water with aggressive magnetic stirring for 1 h, after which acetylacetone was added dropwise into the solution. After stirring for another 20 min, tetrabutyl titanate was injected to produce a solution with a molar ratio of tetrabutyl titanate:P123:HCl:ethyl alcohol:H_2O:acetylacetone = 1:0.01:0.79:12.86:4.89:0.10. After allowing the solution to stand for 24 h, fresh rose petals were added individually into the obtained solution and held for 20 s, then lifted. The fresh rose petals were kept at room temperature for 7 days, then heated to 90 °C for 24 h to strengthen the interaction between the inorganic components. Finally, macro-mesoporous TiO_2 was obtained after calcination at 450 °C in air for 3 h.

2.3. Preparation of the modified electrode

A glassy carbon electrode (GCE, d = 4 mm) was sequentially polished with 2000 mesh metallographic sandpaper and 0.05 μm alumina slurry. It was then washed with ethanol and DI water and dried under a purified nitrogen stream. The prepared TiO_2 was re-suspended in DI water before drop-coating onto the electrode. For this process, 7 μL of a suspension containing 0.1 mg mL^{-1} TiO_2 was applied dropwise onto the electrode to obtain a mesoporous TiO_2-modified electrode (TiO_2/GCE). Electrodeposition of Pt onto the TiO_2/GCE was performed in 5 mM H_2PtCl_6 for 50 s at −0.3 V. After rinsing with DI water, the resulting Pt/TiO_2/GCE

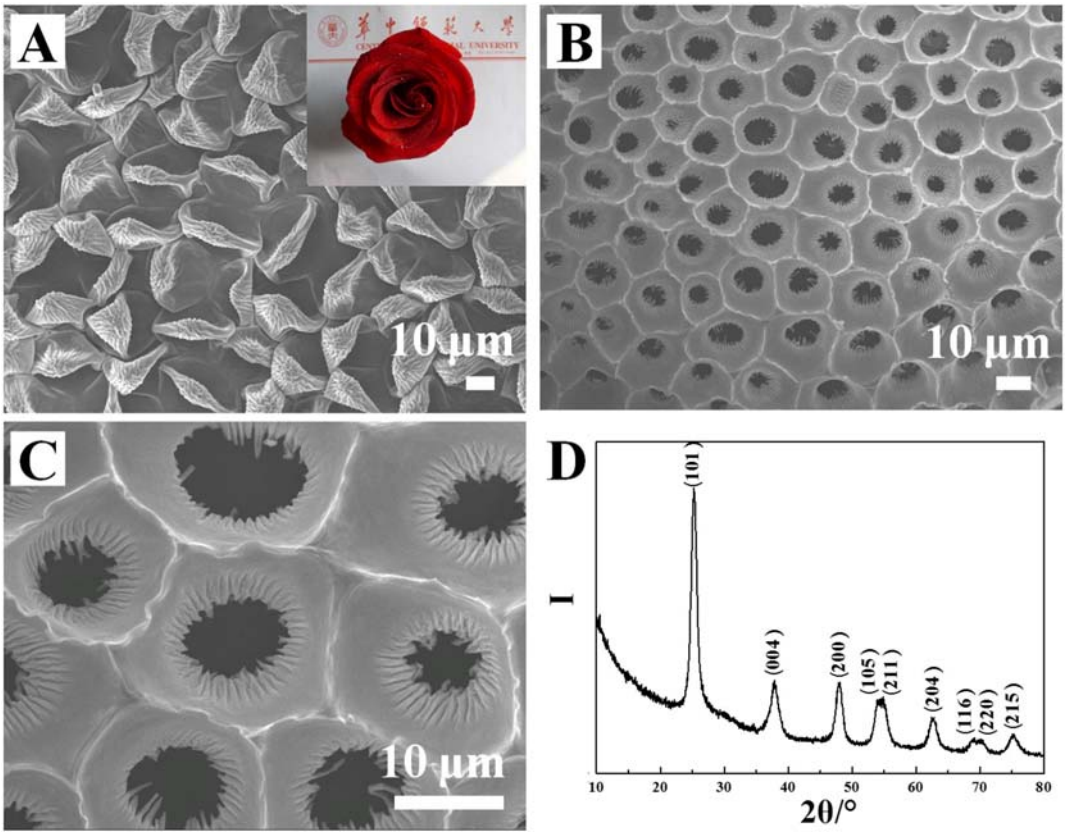

Fig. 1. SEM (A) and optical (inset) images of rose petal; SEM (B and C) images and XRD spectrum (D) of as- prepared macro-mesoporous TiO_2.

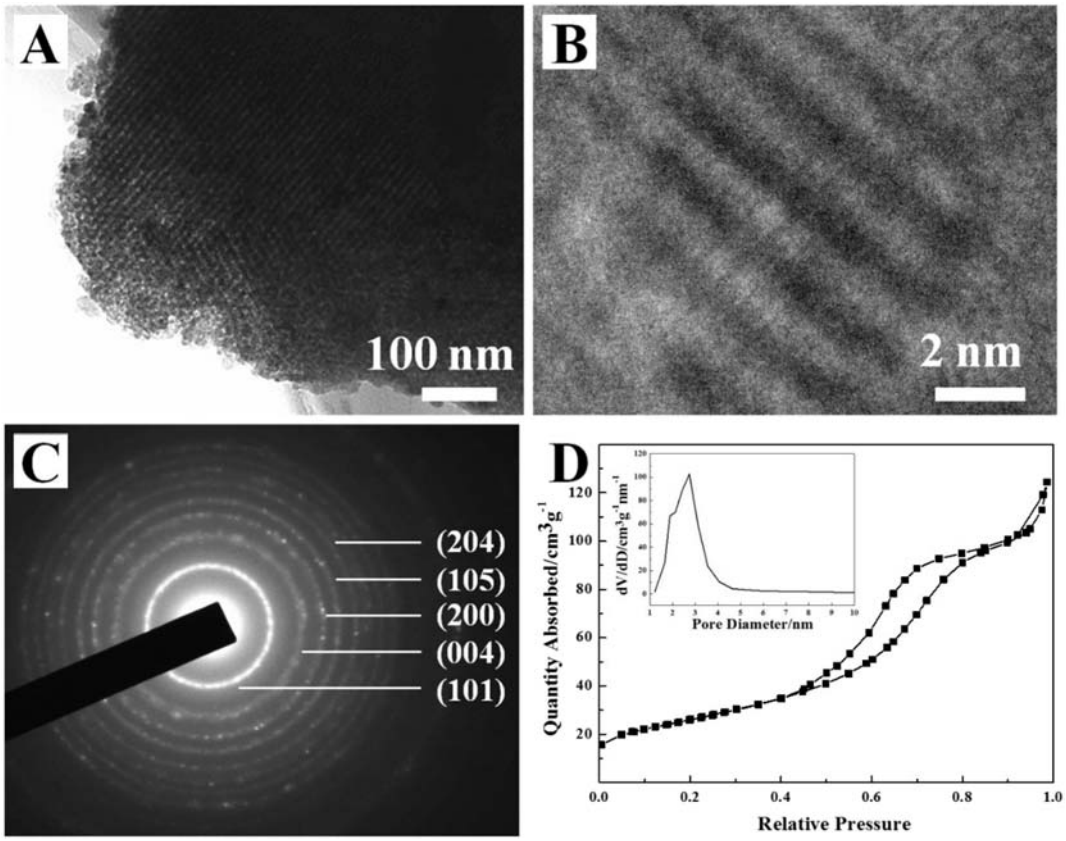

Fig. 2. TEM (A) and HRTEM (B) images, selected area diffraction (C), nitrogen adsorption (ADS)/desorption (DES) isotherms (D), and pore size distribution (inset of D) of as-prepared macro-mesoporous TiO_2.

was incubated in 1 mg mL^{-1} HRP for 12 h. Finally, the prepared electrode was placed in a refrigerator at 4 °C before use.

3. Results and discussion

3.1. Characterization of macro-mesoporous TiO_2

The morphology of the fresh rose petals and the as-prepared macro-mesoporous TiO_2 was investigated by SEM. As shown in the SEM and optical images of the fresh rose petal (Fig. 1A and inset), papillae with an average diameter of 12.6 μm were found on its surface, surrounded by flutes. This special structure allowed a uniform distribution of the precursor solution onto the flutes when the fresh rose petal was dipped into the previously described solution. From the SEM images of the obtained macro-mesoporous TiO_2, shown in Fig. 1B and C, macropores (dark features) with diameters of ~10 μm can be seen, a feature which increases the available surface area and is beneficial to maintaining the highly consistent diameter of the produced mesoporous structure. XRD was also used to examine the prepared TiO_2 sample, and all of the peaks in the resulting pattern (Fig. 1D) were indexed to TiO_2 in anatase form (JCPDS 21–1272).

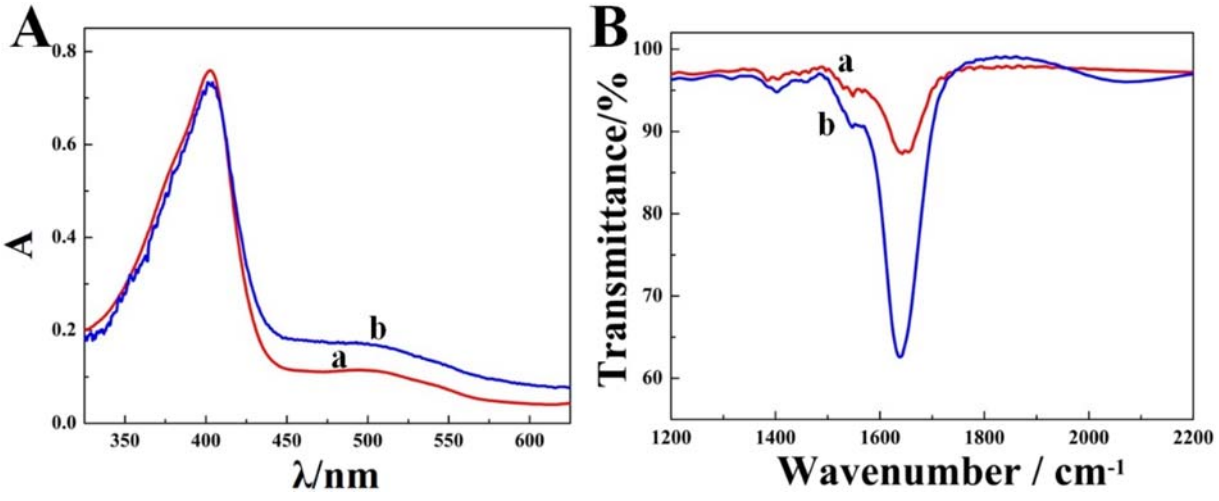

Fig. 3. UV–vis absorption spectra (A) and FT-IR transmittance spectra (B) of (a) HRP and (b) HRP/Pt/TiO_2.

Transmission electron microscopy (TEM) images of the macro-mesoporous TiO_2 are shown in Fig. 2A and B. In these images, ordered columnar mesopores with diameters of ~3 nm can be seen. Selected area electron diffraction (SAED) results for the prepared TiO_2 can be found in Fig. 2C, in which a series of concentric circles indicates the polycrystalline structure of the product, and the corresponding crystal planes are consistent with the XRD result shown in Fig. 1D. Nitrogen adsorption-desorption techniques were also used to investigate the pore structure of the macro-mesoporous TiO_2. As seen from Fig. 2D, the results show a typical type IV isotherm with an H2-type hysteresis loop, suggesting that the average size of the TiO_2 mesopores was 3 nm (inset of Fig. 2D), which is in agreement with the TEM results.

3.2. Spectroscopic results

UV–vis absorption spectroscopy is a sensitive method for investigation of the conformational integrity of proteins via the Soret absorption band, which can be used to test the impact of carriers to the structural integrity of loaded proteins [25]. As seen from Fig. 3A, the Soret band of HRP appears at the wavelength of 403 nm (curve b) after mixing with macro-mesoporous TiO_2 and Pt nanoparticles, which is in the same position as that of native HRP (curve a). This result indicates that due to the good biocompatibility of TiO_2 and Pt nanoparticles, the HRP in the mixture was not denatured and instead retained its native structure.

FT-IR spectroscopy is another powerful tool for monitoring the secondary structure of proteins. Structural information for polypeptide chains can be revealed by examining the infrared absorption bands of amide I and amide II [26]. The amide I band in the position of 1700–1600 cm^{-1} corresponds to the C═O stretching vibration of peptide linkages in the backbone of proteins, while the amide II band located at 1600–1500 cm^{-1} is ascribed to the combination of the N—H in-plane bending and C—N stretching vibrations of peptide groups. Fig. 3B shows that the amide I and amide II bands (1637 cm^{-1} and 1546 cm^{-1}) of HRP in the mixture were almost in the same position as those of native HRP (1643 cm^{-1} and 1548 cm^{-1}).

3.3. Electrochemical characteristics of the modified electrodes

Cyclic voltammograms of TiO_2/GCE and Pt/TiO_2/GCE were obtained in a solution of 0.5 M H_2SO_4. As shown in Fig. 4, hydrogen adsorption/desorption and oxide formation/stripping peaks can be found in the

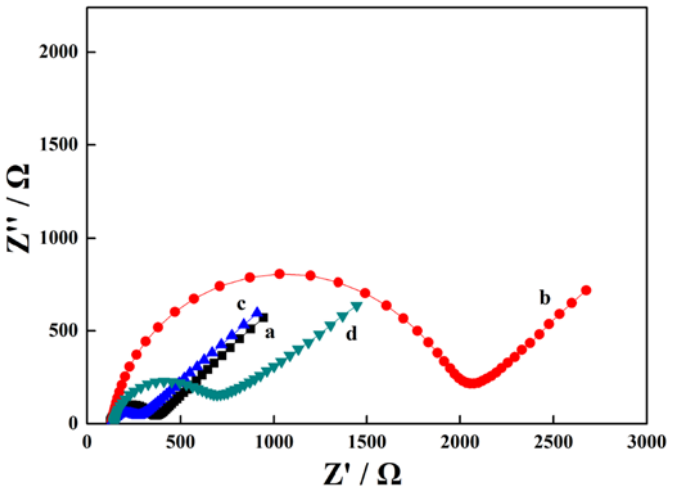

Fig. 5. Electrochemical impedance spectra for (a) GCE, (b) TiO_2/GCE, (c) Pt/TiO_2/GCE and (d) HRP/Pt/TiO_2/GCE in 5 mM $K_3Fe(CN)_6$ /$K_4Fe(CN)_6$ (1:1) containing 0.1 M KCl.

voltammetry results from Pt/TiO_2/GCE (curve b) but are absent in those from TiO_2/GCE (curve a), which indicates the successful loading of Pt nanoparticles [27]. The charge transfer resistance of the different modified electrodes was explored by electrochemical impedance spectroscopy (EIS) in a mixed solution of 5.0 mM $[Fe(CN)_6]^{3-/4-}$ and 0.1 M KCl with a swept frequency range from 10^5 to 0.1 Hz. The resulting Nyquist plots are shown in Fig. 5, in which the diameter of the semi-circule is equal to the electron transfer resistance (R_{et}) and the slope of the linear portion corresponds to the diffusion processes [28]. The R_{et} value of the bare GCE was 264.5 Ω (curve a). The R_{et} value of TiO_2/GCE (curve b) increased to 2141.9 Ω, an effect which was mainly due to the successful immobilization of the poorly conductive macro-mesoporous TiO_2 onto the GCE. After electrochemical deposition of Pt nanoparticles onto the TiO_2-modified electrode, the R_{et} value dramatically decreased to175.9 Ω, indicating the effectiveness of the Pt in increasing the electron transfer rate. Finally, the R_{et} increased to 629.3 Ω after HRP was immobilized onto the electrode.

Fig. 6 exhibits the typical cyclic voltammograms of the different modified electrodes in N_2-saturated 0.1 M PBS (pH 7.0) at a scan rate of 50 mV/s. No peak was observed on the voltammograms produced from the bare GCE (curve a), TiO_2/GCE (curve b) and Pt/TiO_2/GCE (curve c), suggesting that the macro-mesoporous TiO_2, Pt nanoparticles

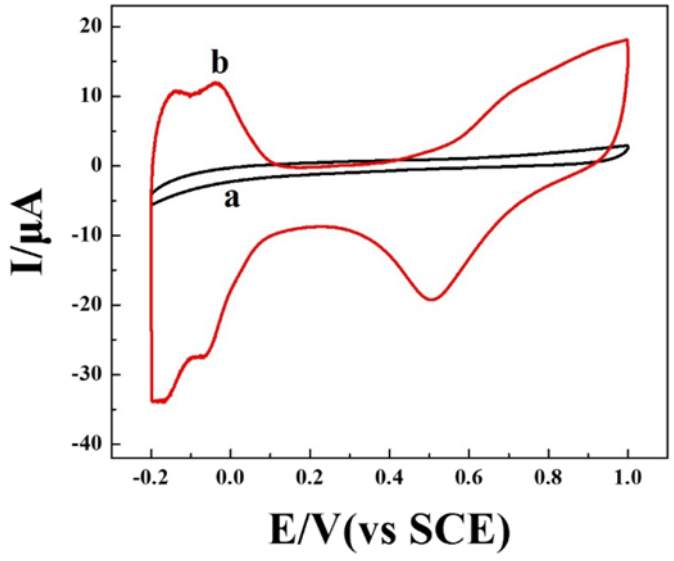

Fig. 4. Cyclic voltammograms of (a) TiO_2/GCE and (b) Pt/TiO_2/GCE electrodes in 0.5 M H_2SO_4 at a scan rate of 50 mV/s.

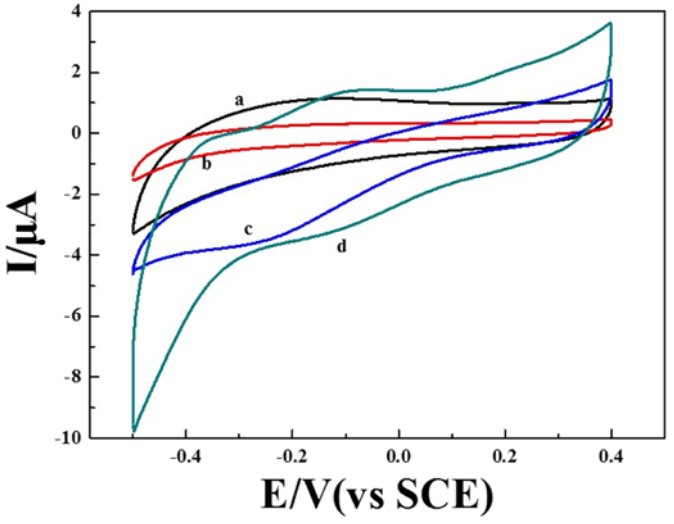

Fig. 6. Cyclic voltammograms of (a) bare GCE, (b) TiO_2/GCE, (c) Pt/TiO_2/GCE, and (d) HRP/Pt/TiO_2/GCE in 0.1 M PBS (pH 7.0).

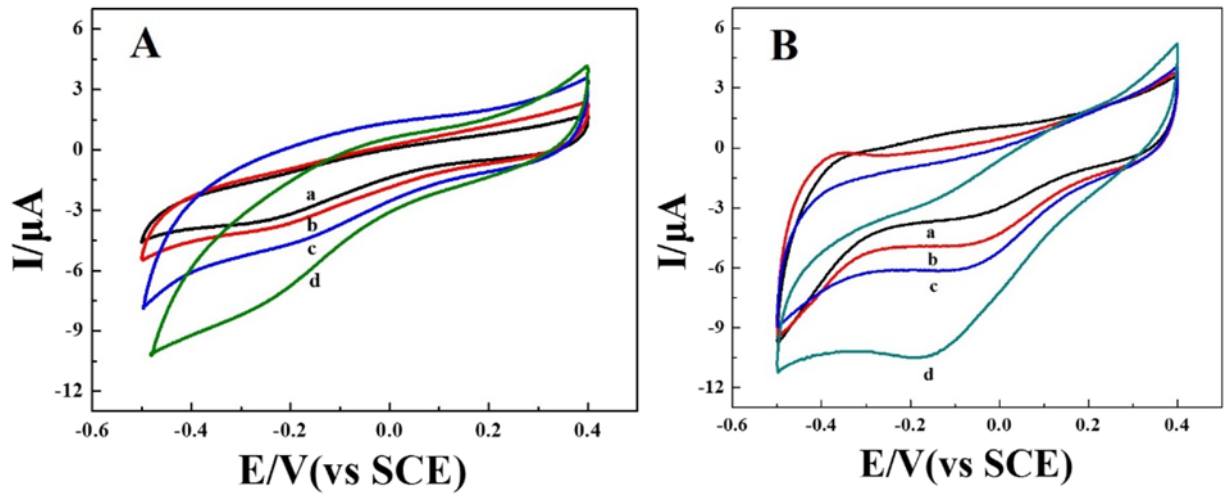

Fig. 7. Cyclic voltammograms of (A) Pt/TiO_2/GCE and (B) HRP/Pt/TiO_2/GCE in 0.1 M PBS (pH 7.0) in the (a) absence and presence of (b) 1 mM, (c) 2 mM and (d) 9 mM H_2O_2.

and their mixture are all electrically inactive. In contrast, the voltammogram produced from the HRP/Pt/TiO_2/GCE yielded two reversible peaks (curve d), which indicated the successful immobilization of HRP onto the electrode with its native structure maintained, allowing direct electron transfer between the HRP and the electrode.

3.4. Electrochemical response of the HRP/Pt/TiO_2/GCE to H_2O_2

The electrochemical catalysis of H_2O_2 by the Pt/TiO_2/GCE and HRP/Pt/TiO_2/GCE in 0.1 M PBS (pH 7.0) is displayed in Fig. 7A and B. With increasing concentrations of H_2O_2, the Pt/TiO_2/GCE and HRP/Pt/TiO_2/GCE reduction peaks also increased, revealing that both Pt and HRP/Pt can electrochemically reduce H_2O_2. The increase in the reduction current of HRP/Pt/TiO_2/GCE (Fig. 7 B) was much greater than that of HRP/Pt/TiO_2/GCE (Fig. 7 A), particularly at −0.2 V, suggesting that the immobilized HRP retained its ability to electrochemically reduce H_2O_2 and that the performance of the modified electrode can thereby be promoted with its presence.

Fig. 8 shows a typical current-time response of the HRP/Pt/TiO_2/GCE at −0.2 V with the addition of H_2O_2. The current increased dramatically when H_2O_2 was injected into an electrochemical cell containing 0.1 M PBS, and a steady-state current was achieved within 3 s. The linear regression equation for the HRP/Pt/TiO_2/GCE biosensor was obtained from the calibration curve (inset of Fig. 8) as I (μA) = −0.074 − 1.256 c (mmol L^{-1}), and the correlation coefficient was calculated to be 0.999 (n = 16). The linear detection range was 5 μM to 8 mM with a detecting limit of 1.65 μM (3σ). The performances of various H_2O_2 biosensors based on different TiO_2 nanomaterials [29–32] are shown in Table 1. From the comparison of these performance parameters, it can be concluded that the developed electrode exhibits the good characteristics of a shorter response time, a wider linear range and a lower detection limit.

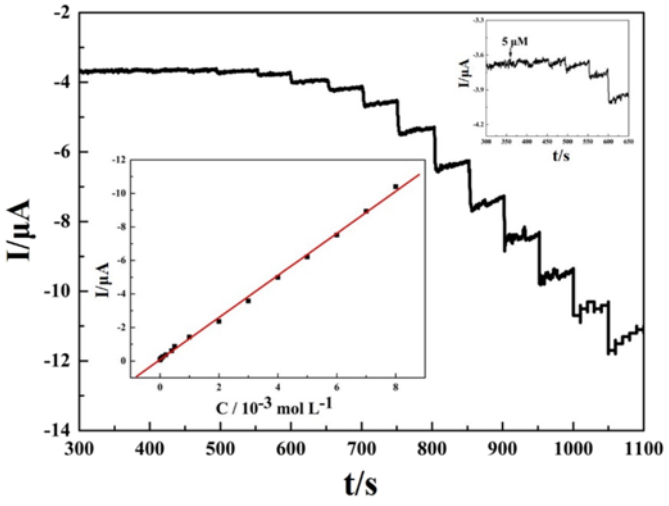

Fig. 8. Chronoamperometric response of the HRP/Pt/TiO_2/GCE in 0.1 M PBS (pH 7.0) at an applied potential of −0.2 V and the calibration curve resulting from different concentrations of H_2O_2.

Differential pulse voltammetry (DPV) of the HRP/Pt/TiO_2/GCE was also carried out to examine its catalytic performance. The DPV results in 0.1 M PBS with different concentrations of H_2O_2 are displayed in Fig. 9A, and the data indicate a good catalytic behaviour. From the relationship between the peak currents and the concentrations of H_2O_2 (Fig. 9B), the linear regression equation of the HRP/Pt/TiO_2/GCE biosensor was obtained as I (μA) = −0.314–1.579 c (mmol L^{-1}) between 0 and 4 mM, with a low detection limit of 1.36 μM. These results further demonstrate the good performance of the proposed biosensor.

3.5. Stability, reproducibility and selectivity

Cyclic voltammetry was also applied to demonstrate the stability of the HRP/Pt/TiO_2/GCE. The peak current decreased only 1.6% compared to the initial peak current over 50 cycles. After storage in 0.1 M PBS at 4 °C for one month, the peak current of the HRP/Pt/TiO_2/GCE still remained at 90.7% of the initial peak current, confirming that the as-prepared biosensor is stable in PBS. The reproducibility of the HRP/Pt/TiO_2/GCE was investigated by using six different electrodes to detect a

Table 1
Comparison of the performances of various H_2O_2 biosensors based on different TiO_2 nanomaterials.

	Linear range (μM)	Detection limit (μM)	Response time (s)	References
HRP/RTIL/GNPs-TNTs/Nafion electrode	5–1000	2.1	4	[29]
Thiolated HRP gold nanoparticle-PTA-TiO_2 nanotube/[Demim]Br/nafion-coated electrode	65–1600	5		[30]
Nafion/HRP–GNSs–TiO_2/GCE	41–630	5.9	3	[31]
HRP/Au/TiO_2 nanotube arrays/Ti	5–400	2	5	[32]
HRP/Pt/TiO_2/GCE	5–8000	1.36	3	Present work

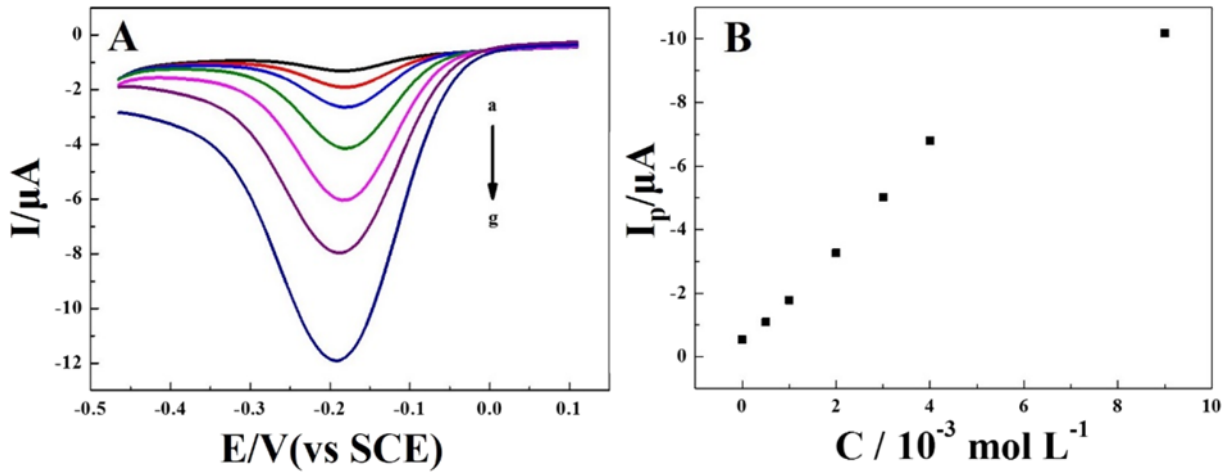

Fig. 9. (A) Differential pulse voltammetry of the HRP/Pt/TiO_2/GCE in 0.1 M PBS (pH 7.0) with (a) 0 mM, (b) 0.5 mM, (c) 1 mM, (d) 2 mM, (e) 3 mM, (f) 4 mM and (g) 9 mM concentrations of H_2O_2 and (B) the relationship between the peak currents and the concentration of H_2O_2.

1 mM concentration of H_2O_2, and the resulting relative standard deviation (RSD) of the detection results was 3.1%. Finally, we also studied the selectivity of the HRP/Pt/TiO_2/GCE using chronoamperometry. As shown in Fig. 10, there was no change when interferents including glucose, $NaNO_3$, AA and UA (1 mM) were added into the electrochemical cell, proving that the developed biosensor has a high selectivity for the detection of H_2O_2.

4. Conclusions

In summary, fresh rose petals and P123 were used as templates to prepare highly ordered macro-mesoporous TiO_2 via a simple, facile and controllable dual-template method. The prepared TiO_2 was in anatase form, and the diameters of the macropores and mesopores were 10 μm and 3 nm, respectively. These structural features can efficiently improve the specific surface area of TiO_2 to provide more active sites for the immobilization of noble metals and biomolecules. From the TiO_2 material, a novel H_2O_2 biosensor was developed with a wider linear range, lower detection limit, good stability and high selectivity, based on the good biocompatibility and high surface area of TiO_2 together with the good conductivity of Pt nanoparticles. It is believed that the as-prepared macro-mesoporous TiO_2 can also be used to produce other enzyme-based biosensors.

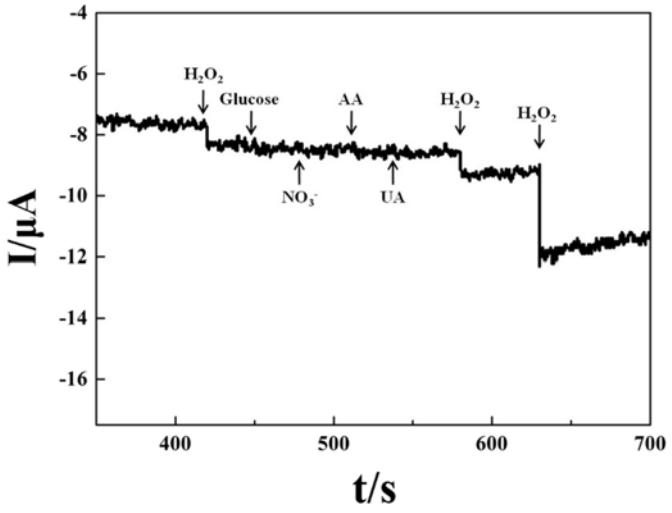

Fig. 10. Chronoamperometric curves of the HRP/Pt/TiO_2/GCE in 0.1 M PBS (pH 7.0) after successive additions of 0.5 mM H_2O_2, 1 mM glucose, 1 mM NO_3^-, 1 mM AA, 1 mM UA, 0.5 mM H_2O_2 and 2 mM H_2O_2.

Acknowledgments

This work was supported by the National Natural Science Foundation of China (21475115), Program for University Innovative Research Team of Henan (15IRTSTHN001), Henan Provincial Science and technology innovation team (C20150026), Nanhu Scholars Program of XYNU, Nanhu Scholars Program for Young Scholars of XYNU, Natural Science Foundation of Henan Province (162300410230), Henan Science and Technology Cooperation Project (172106000064), and Research Starting Foundation for High Level Talent of XYNU.

References

[1] V. Boffa, Y.Z. Yue, W. He, Sol—gel synthesis of a biotemplated inorganic photocatalyst: a simple experiment for introducing undergraduate students to materials chemistry, J. Chem. Educ. 89 (2012) 1466–1469.
[2] P. Si, S.J. Ding, J. Yuan, X.W. Lou (David), D.H. Kim, hierarchically structured one-dimensional TiO_2 for protein immobilization, direct electrochemistry, and mediator-free glucose sensing, ACS Nano 5 (2011) 7617–7626.
[3] Y. Zhang, P.L. He, N.F. Hu, Horseradish peroxidase immobilized in TiO_2 nanoparticle films on pyrolytic graphite electrodes: direct electrochemistry and bioelectrocatalysis, Electrochim. Acta 49 (2004) 1981–1988.
[4] D.L. Yu, X.F. Zhu, Z. Xu, X.M. Zhong, Q.F. Gui, Y. Song, S.Y. Zhang, X.Y. Chen, D.D. Li, Facile method to enhance the adhesion of TiO_2 nanotube arrays to Ti substrate, ACS Appl. Mater. Interfaces 6 (2014) 8001–8005.
[5] J.H. Yu, H.X. Ju, Preparation of porous titania sol-gel matrix for immobilization of horseradish peroxidase by a vapor deposition method, Anal. Chem. 74 (2002) 3579–3583.
[6] Z.D. Gao, F.F. Guan, C.Y. Li, H.F. Liu, Y.Y. Song, Signal-amplified platform for electrochemical immunosensor based on TiO_2 nanotube arrays using a HRP tagged antibody-Au nanoparticles as probe, Biosens. Bioelectron. 41 (2013) 771–775.
[7] (a) J. Zhu, X.Q. Liu, X.H. Wang, X.H. Huo, R. Yan, Preparation of polyaniline–TiO_2 nanotube composite for the development of electrochemical biosensors, Sens. Actuators B 221 (2015) 450–457;
(b) J.C. Cardoso, C.A. Grimes, X. Feng, X. Zhang, S. Komarneni, M.V.B. Zanoni, N. Bao, Fabrication of coaxial TiO_2/Sb_2S_3 nanowire hybrids for efficient nanostructured organic–inorganic thin film photovoltaics, Chem. Commun. 48 (2012) 2818.
[8] M. Ongaro, A. Mardegan, A.M. Stortini, M. Signoretto, P. Ugo, Arrays of templated TiO_2 nanofibres as improved photoanodes for water splitting under visible light, Nanotechnology 26 (2015) 165402.
[9] M. Xu, P.M. Da, H.Y. Wu, D.Y. Zhao, G.F. Zheng, Controlled Sn-doping in TiO_2 nanowire photoanodes with enhanced photoelectrochemical conversion, Nano Lett. 12 (2012) 1503–1508.
[10] Z.H. Yang, Y. Tang, J. Li, Y.C. Zhang, X.Y. Hu, Facile synthesis of tetragonal columnar-shaped TiO_2 nanorods for the construction of sensitive electrochemical glucose biosensor, Biosens. Bioelectron. 54 (2014) 528–533.
[11] H. Liu, K. Guo, C.Y. Duan, X.N. Dong, J.J. Gao, Hollow TiO_2 modified reduced graphene oxide microspheres encapsulating hemoglobin for a mediator-free biosensor, Biosens. Bioelectron. 87 (2017) 473–479.

[12] L.P. Liu, J. Hensel, R.C. Fitzmorris, Y.D. Li, J.Z. Zhang, Preparation and photoelectrochemical properties of CdSe/TiO_2 hybrid mesoporous structures, J. Phys. Chem. Lett. 1 (2010) 155–160.
[13] W. Li, Z.X. Wu, J.X. Wang, A.A. Elzatahry, D.Y. Zhao, A. Perspective, On mesoporous TiO_2 materials, Chem. Mater. 26 (2014) 287–298.
[14] L.F. Zhao, Q. Wei, H. Wu, J.K. Dou, H. Li, Ionic liquid functionalized grapheme based immunosensor for sensitive detection of carbohydrate antigen 15-3 integrated with Cd^{2+} —functionalized nanoporous TiO_2 as labels, Biosens. Bioelectron. 59 (2014) 75–80.
[15] Q.Q. Yang, S.M. Zhu, W.H. Peng, C. Yin, W.L. Wang, J.J. Gu, W. Zhang, J. Ma, T. Deng, C.L. Feng, D. Zhang, Bioinspired fabrication of hierarchically structured, pH-tunable photonic crystals with unique transition, ACS Nano 7 (2013) 4911–4918.
[16] G. Xiao, X. Huang, X.P. Liao, B. Shi, One-pot facile synthesis of cerium-doped TiO_2 mesoporous nanofibers using collagen fiber as the biotemplate and its application in visible light photocatalysis, J. Phys. Chem. C 117 (2013) 9739–9746.
[17] M. Liang, R.X. Su, R.L. Huang, W. Qi, Y.J. Yu, L.B. Wang, Z.M. He, Facile in situ synthesis of silver nanoparticles on procyanidin-grafted eggshell membrane and their catalytic properties, ACS Appl. Mater. Interfaces 6 (2014) 4638–4649.
[18] Y. Xia, Z. Xiao, X. Dou, H. Huang, X.H. Lu, R.J. Yan, Y.P. Gan, W.J. Zhu, J.P. Tu, W.K. Zhang, X.Y. Tao, Green and facile fabrication of hollow porous MnO/C microspheres from microalgaes for lithium-ion batteries, ACS Nano 7 (2013) 7083–7092.
[19] M.A. Mohamed, W.N.W. Salleh, J. Jaafar, M.S. Rosmi, Z.A.M. Hir, M.A. Mutalib, A.F. Ismail, M. Tanemurae, Carbon as amorphous shell and interstitial dopant in mesoporous rutile TiO_2: bio-template assisted sol-gel synthesis and photocatalytic activity, Appl. Surf. Sci. 393 (2017) 46–59.
[20] Z.L. He, W.X. Que, Y.C. He, Synthesis and characterization of bioinspired hierarchical mesoporous TiO_2 photocatalysts, Mater. Lett. 94 (2013) 136–139.
[21] S.H. Yan, S.Y. Ma, X.L. Xu, Y. Lu, H.Q. Bian, X.Y. Liang, W.X. Jin, H.M. Yang, Synthesis and gas sensing application of porous CeO_2–ZnO hollow fibers using cotton as biotemplates, Mater. Lett. 165 (2016) 9–13.
[22] J.L. Song, G.S. Fu, Q. Cheng, Y.C. Jin, Bimodal mesoporous silica nanotubes fabricated by dual templates of CTAB and bare nanocrystalline cellulose, Ind. Eng. Chem. Res. 53 (2014) 708–714.
[23] Y.Y. Zhang, R. Yuan, Y.Q. Chai, Y. Xiang, C.L. Hong, X.Q. Ran, An amperometric hydrogen peroxide biosensor based on the immobilization of HRP on multi-walled carbon nanotubes/electro-copolymerized nano-Pt-poly(neutral red) composite membrane, Biochem. Eng. J. 51 (2010) 102–109.
[24] B. Li, J.Q. Zhao, J. Liu, X.Y. Shen, S.B. Mo, H. Tong, Bio-templated synthesis of hierarchically ordered macro-mesoporous anatase titanium dioxide flakes with high photocatalytic activity, RSC Adv. 5 (2015) 15572–15578.
[25] S.F. Wang, T. Chen, Z.L. Zhang, D.W. Pang, K.Y. Wong, Effects of hydrophilic room-temperature ionic liquid 1-butyl-3-methylimidazolium tetra-fluoroborate on direct electrochemistry and bioelectrocatalysis of heme proteins entrapped in agarose hydrogel films, Electrochem. Commun. 9 (2007) 1709–1714.
[26] Y.P. Song, M.C. Petty, J. Yarwood, W.J. Feast, J. Tsibouklis, S. Mukherjee, Fourier transform infrared studies of molecular ordering and interactions in langmuir-blodgett films containing nitrostilbene and stearic acid, Langmuir 8 (1992) 257–261.
[27] H.C. Gao, F. Xiao, C.B. Ching, H.W. Duan, One-step electrochemical synthesis of PtNi nanoparticle-graphene nanocomposites for nonenzymatic amperometric glucose detection, ACS Appl. Mater. Interfaces 3 (2011) 3049–3057.
[28] O. Parlak, A. Tiwari, A.P.F. Turner, A. Tiwari, Template-directed hierarchical self-assembly of graphene based hybrid structure for electrochemical biosensing, Biosens. Bioelectron. 49 (2013) 53–62.
[29] X.Q. Liu, H.Q. Feng, R.X. Zhao, Y.B. Wang, X.H. Liu, A novel approach to construct a horseradish peroxidase|hydrophilic ionic liquids|au nanoparticles dotted titanate nanotubes biosensor for amperometric sensing of hydrogen peroxide, Biosens. Bioelectron. 31 (2012) 101–104.
[30] X.Q. Liu, J.M. Zhang, S.H. Liu, Q.Y. Zhang, X.H. Liu, D.K.Y. Wong, Gold nanoparticle encapsulated-tubular TIO_2 nanocluster as a scaffold for development of thiolated enzyme biosensors, Anal. Chem. 85 (2013) 4350–4356.
[31] Y. Wang, X.L. Ma, Y. Wen, Y.Y. Xing, Z.R. Zhang, H.F. Yang, Direct electrochemistry and bioelectrocatalysis of horseradish peroxidase based on gold nano-seeds dotted TiO_2 nanocomposite, Biosens. Bioelectron. 25 (2010) 2442–2446.
[32] A.K.M. Kafi, G.S. Wu, A.C. Chen, A novel hydrogen peroxide biosensor based on the immobilization of horseradish peroxidase onto au-modified titanium dioxide nanotube arrays, Biosens. Bioelectron. 24 (2008) 566–571.